Int. J. Electrochem. Sci., 7 **(2012)** 10923 - 10932

International Journal of
ELECTROCHEMICAL
SCIENCE
www.electrochemsci.org

An improved Carbon-Coating Method for $LiFePO_4$/C composite derived from Fe^{3+} precursor

Rui Rui Zhao[1], *Guo Zheng Ma*[1], *Li Cai Zhu*[1], *Ai Ju Li*[1], *Hong Yu Chen*[1, 2,*]

[1] School of Chemistry and Environment, South China Normal University, Guangzhou 510006, PR China
[2] Base of Production, Education & Research on Energy Storage and Power Battery of Guangdong Higher Education Institutes, Guangzhou 510006, PR China
[*]E-mail: battery_chy@126.com, hychen@scnu.edu.cn

Received: 7 September 2012 / *Accepted:* 10 October 2012 / *Published:* 1 November 2012

In this paper, a novel hydroxyethylcellulose (HEC)-assisted carbon-coating method was developed to synthesize $LiFePO_4$/C composites. The structure and morphological transformation of the as-prepared samples were studied using a combination of X-ray diffraction, scanning electron microscopy, transmission electron microscopy, and Raman spectroscopy. The particles of the samples obtained were more homogeneous than the reference sample prepared without the addition of HEC and the coated carbon were more uniformly distributed on the $LiFePO_4$ surface. In addition, the HEC-assisted sample exhibited higher capacities and better rate capability in the charge-discharge test, and the charge transfer resistance calculated from the electrochemical impedance spectra data was smaller.

Keywords: hydroxyethylcellulose, $LiFePO_4$, cathode, Li-ion batteries

1. INTRODUCTION

The demand for batteries with improved specific capacity and high energy density has promoted research on lithium ion battery cathodes and lithium ion phosphate ($LiFePO_4$), which were discovered by Goodenough in 1997 [1]. This research niche has gained enormous attention due to the low cost, high theoretical capacity, and environmental benignity of the material [2,3]. However, its main shortcomings include poor electronic conductivity and limited lithium ion diffusion coefficiency. The electronic conductivity of $LiFePO_4$ is about 10^{-9} S cm^{-1} at room temperature and around 10^{-3} S cm^{-1} and 10^{-5} S cm^{-1} for $LiCoO_2$ and $LiMn_2O_4$, respectively [4]. Many efforts have been made to overcome these limitations, including doping with other cations [5,6], coating particles with electronically

conductive agents, such as carbon [7] and silver [8], or decreasing the particle size [9]. These strategies have improved the electrochemical performance of lithium ion significantly.

Using ferric iron as the precursor for $LiFePO_4$ synthesis can simplify the process and decrease costs, considering that the need for inert gas is reduced. However, the reduction agent remains indispensable in the heat treatment process. The most commonly used reduction agents are organisms that can produce gases, such as hydrogen (H_2), or gaseous hydrocarbons during their calcination [10], thereby reducing Fe^{3+} to Fe^{2+}. In addition, decomposition of the organism can result in the formation of carbonaceous deposits on the surface of the $LiFePO_4$ particles. Peng et al. [11] employed oxalic acid as reductant to obtain a $LiFePO_4$/C composite with excellent performance from $FePO_4 \cdot 2H_2O$. Yang et al. [12] prepared $LiFePO_4$/C using glucose as a reducing agent and $FePO_4.2H_2O$ as an iron source. Different organic acid molecules feature various decomposition mechanisms to form reducing intermediates, which can influence the properties of the $LiFePO_4$ composites obtained [13]. Thus, a complex carbon source may play a synergistic effect in $LiFePO_4$ synthesis, as reported by Hong et al. [14], who also observed that the morphology and electrochemical performance of the composites could be optimized by changing the ratio of sucrose to citric acid. Oh et al. [15] synthesized double carbon-coated $LiFePO_4$ with sucrose and pitch as the carbon source and reducing agent, respectively. Other reducing agents have also been used. Wang et al. [16] synthesized $LiFePO_4$/C from $FePO_4 \cdot 4H_2O$ through a solid-liquid phase reaction using $(NH_4)_2SO_3$ as a reducing agent. The particle size of the obtained sample ranged from 100 nm to 300 nm.

Various synthesis methods for preparing $LiFePO_4$ have been proposed, such as solid-state reaction [17], sol-gel technique [18], hydrothermal synthesis [19], and so on. Of these, the solid-state reaction method can adequately meet commercial manufacture requirements. In the solid-state method, pre-mixing the precursors is crucial in obtaining an end product with superior performance. The rheological phase method can produce well-dispersed mixtures to facilitate the interaction between the precursor particles within a relatively large volume of solvent. Some researchers even use this method to mix precursors without the need for ball-milling [14]. However, a layering problem may occur during the drying process, given that the mixture is in rheological phase.

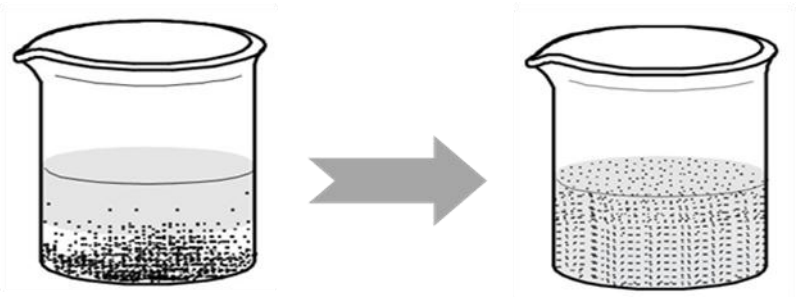

Figure 1. Diagram of the possible effect of HEC.

In the present study, we present a novel hydroxyethylcellulose (HEC)-assisted rheological phase method for synthesizing$LiFePO_4$/C composites. Custom-made $FePO_4$ was used as the iron

source. We expect that the high viscosity of HEC can prevent precursor loss during the drying process when the rheological phase method is used, as shown in Fig. 1, and may help impede the agglomeration of $LiFePO_4$ particles.

2. EXPERIMENTAL

2.1. Preparation of $LiFePO_4$/C

Amorphous $FePO_4$ was obtained as previous reference reported [20]. 100ml solution containing 0.03mol $FeCl_3$ was slowly added to another 100ml 0.03 $NH_4H_2PO_4$ and 1ml Tween#80-containing solution; the whole reaction vessel was placed in a water bath with a constant temperature of 60°C and the pH value of the solution was adjusted to 2.5. The obtained precipitate by centrifugation was dried in the oven and preheated at 400°C for 6 h in the air to get anhydrous $FePO_4$ before use.

The $LiFePO_4$/C composites were synthesized by a rheological phase method. Stoichiometric proportions of $FePO_4$, Li_2CO_3 (Aladdin, Shanghai), and 16 wt.% sucrose were added to the HEC solution to form a slurry, which was subsequently ball-milled for 5 h. The HEC solution was obtained by dissolving HEC powder (Aladdin, Shanghai) in deionized water over a water bath. The mass ratio of HEC to the precursor used was 4 wt.%. The whole mixture was dried under vacuum conditions heated at 400 °C for 4 h under an argon (Ar) atmosphere, and cooled to room temperature. The precipitate obtained was ground for another 1 h and sintered at 600 °C under a 5% H_2/Ar atmosphere for 10 h to obtain the final $LiFePO_4$/C samples. The samples were labeled "SSH."

For comparison, another sample was prepared with 20 wt.% sucrose as the carbon source. The $LiFePO_4$/C was prepared following the same procedure described earlier. This sample was obtained labeled "SS."

2.2. Characterization

X-ray diffraction (XRD) of the powders was carried out with a Bruker D8 X-ray diffractometer in the range $15°<2\theta<80°$ using Cu Kα radiation (λ=0.12418 nm). The particle size and morphology of the samples were observed with a Philips XL-60 scanning electron microscope (SEM). The properties of the coated carbon were studied in more detail by high-resolution transmission electron microscopy (HRTEM; JEM-2010 transmission electron microscope) and Raman spectroscopy using a Raman scattering spectrometer (Renishaw-Ramascope).

2.3. Electrochemical measurements

For electrochemical characterization, the synthesized material, acetylene black, and polyvinylidene fluoride (80:10:10) were mixed in *N*-methylpyrrolidinone to prepare a slurry. The resulting slurry was then coated onto an aluminum foil and dried for 10 h in a vacuum oven at 120 °C. The lithium metal was used as the anode, Celgard 2320 was used as the separator, and 1 M $LiPF_6$ in

EC:DEC:EMC=1:1:1 was used as the electrolyte. The 2025-type coin cells were assembled in an Ar-filled dry glove box.

The charge/discharge and cycling properties of the coin cells were conducted on a Neware Battery Test System with a galvanostatic charge/discharge at different C- rates in the voltage range of 2.5 V to 4.2 V (versus Li/Li^+) under a constant temperature of 25 °C. Electrochemical impedance spectroscopy (EIS) was employed to characterize the resistance of the cathode materials under an open-circuit potential state after 10 cycles on an Autolab electrochemical workstation (USA). The frequency ranged from 10^{-1} Hz to 10^5 Hz, and the amplitude of the overpotential was 0.005 V.

3. RESULTS AND DISCUSSION

3.1 Structure and morphology analysis

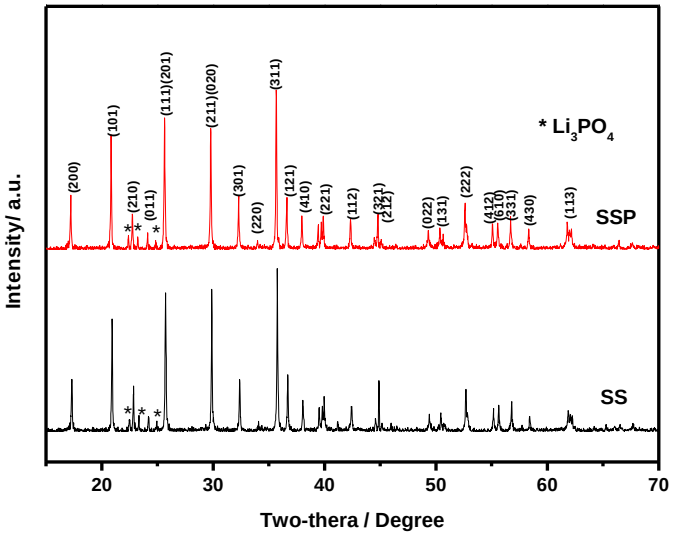

Figure 2. XRD patterns of the samples. The reflections marked with * refer to the impurity phase, Li_3PO_4.

Fig. 2 depicts the XRD patterns of the two as-prepared $LiFePO_4$/C samples. The spectra show the presence of the olivine-like-structured $LiFePO_4$ as the major crystalline phase, as well as a secondary phase (Li_3PO_4). No significant difference was found between the two samples based on the patterns. The least squares fit of the XRD data yielded lattice parameter values of a=10.332, b=6.013, and c=4.659 for the SS sample and a=10.329, b=6.012, and c=4.650 for the SSH sample. The average grain size estimated using the Scherrer formula was found to be around 50 nm to 70 nm and 20 nm to 30 nm for the SS and SSH samples, respectively.

Figs. 3a to 3d show the particle morphologies of the as-prepared $LiFePO_4$/C materials as revealed by SEM. The primary particles of both samples presented ellipsoid-like shapes. The SS

sample consisted of primary particles of about 200 nm, as well as some large agglomerates of up to a few microns in size. In contrast, the SSH composite showed a more regular particle size distribution with fewer agglomerations compared with the SS sample. The diameter of the SSH particles ranged from 50 nm to 200 nm. A smaller particle size can help reduce the diffusion length in the composite cathode and improve the ionic diffusivity accordingly. The SEM results confirm that HEC plays an important role in sample dispersion and agglomeration reduction.

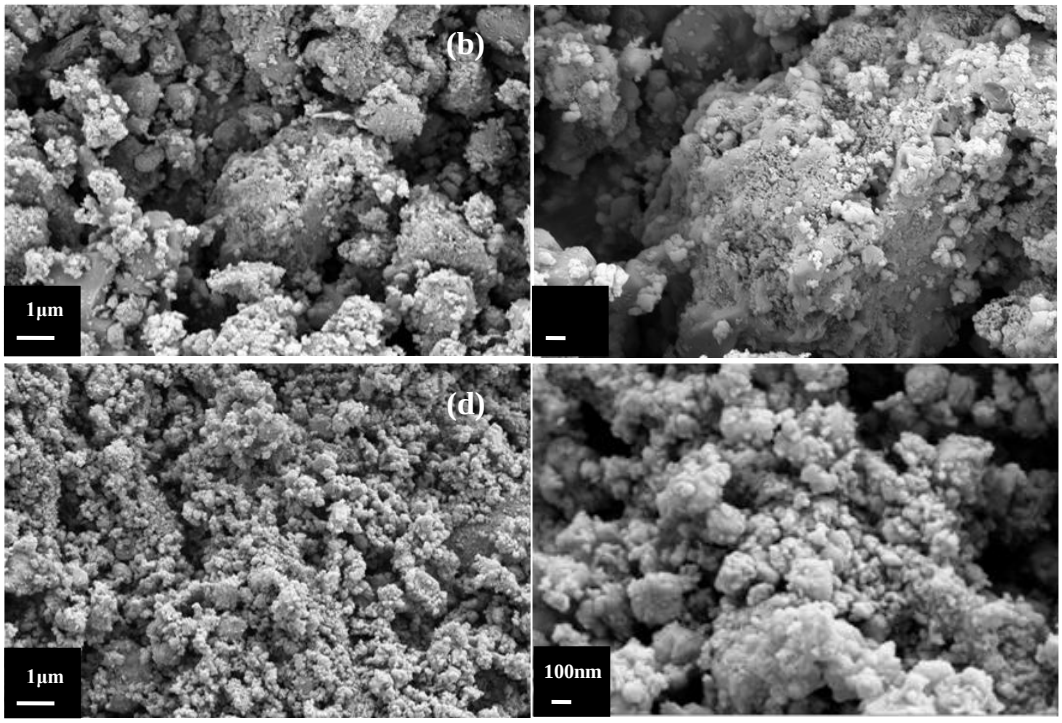

Figure 3. SEM images of (a, b) the SS sample and (c, d) the SSH sample.

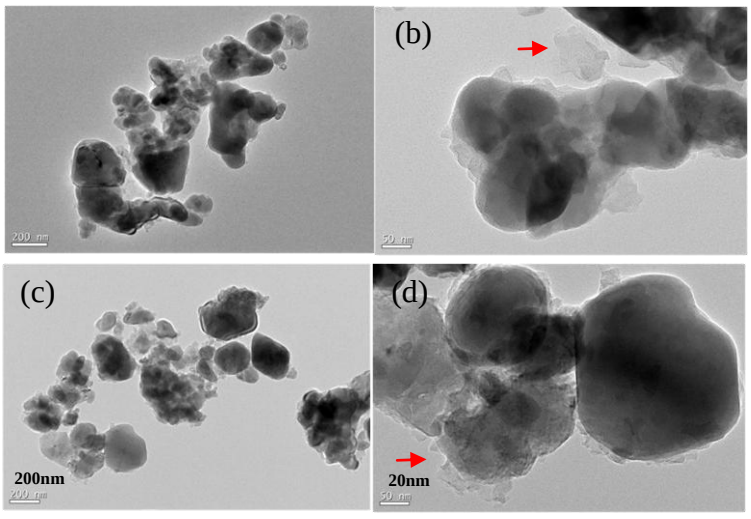

Figure 4. TEM micrographs of (a, b) the SS sample and (c, d) the SSH sample.

Considering that sucrose can be dissolved in water, other precursors of the SS sample, which use sucrose solely as both the carbon source and reducing agent, may be reduced during the drying process and separated from the sucrose. For the SSH sample, the precursors can be wrapped in the HEC-sucrose network during the drying process, resulting in well-dispersed particles and a uniform carbon coating, which the TEM images further confirm.

Detailed features of the carbon coating on the $LiFePO_4$ surface can be observed from the HRTEM images, as shown in Figs. 4a to 4d. The relatively dark portion shown in the images is $LiFePO_4$ and the light gray part is carbon. In the SSH images, the carbon surrounds $LiFePO_4$ crystal grains like a web, which can improve the electronic conductivity of the materials. The thickness of the carbon coating is less than 5 nm, which would not impede lithium diffusion. However, for the SS sample, carbon patches can be observed, as indicated by arrows.

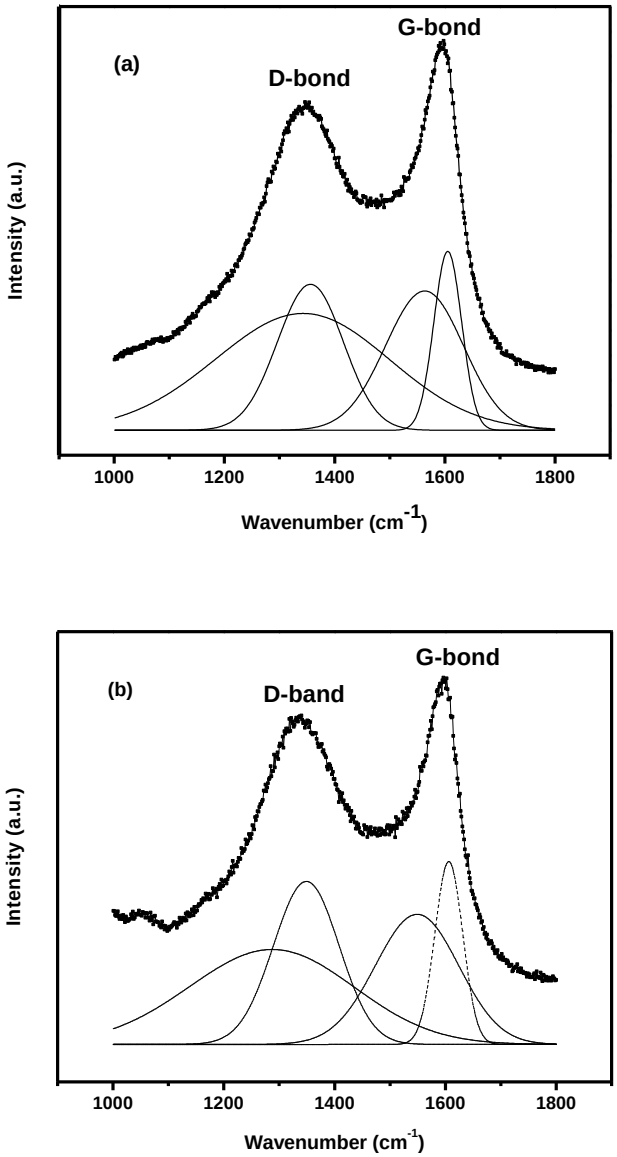

Figure 5. Raman spectra and fittings of the samples.

Raman spectroscopy is an effective tool for confirming the presence of amorphous carbon present in the $LiFePO_4$/C composite cathode, as well as its carbon properties. Fig. 5 shows the Raman spectrum of the $LiFePO_4$/C composite samples. The typical D and G bonds of carbon appeared around 1340 cm^{-1} and 1580 cm^{-1}, respectively. The G bond is assigned to the E_{2g} graphite mode, while the D band is associated with A_{1g}, which is related to the breakage of symmetry at the edges of graphite sheets [21]. The relative intensity ratio, $R=I_G/I_D$, defines the level of order and in-plane crystal size for pyrolytic carbon. A high R indicates the presence of a larger amount of graphene carbon compared with the disordered carbon structure, which can improve the electrical conductivity of $LiFePO_4$ powders.

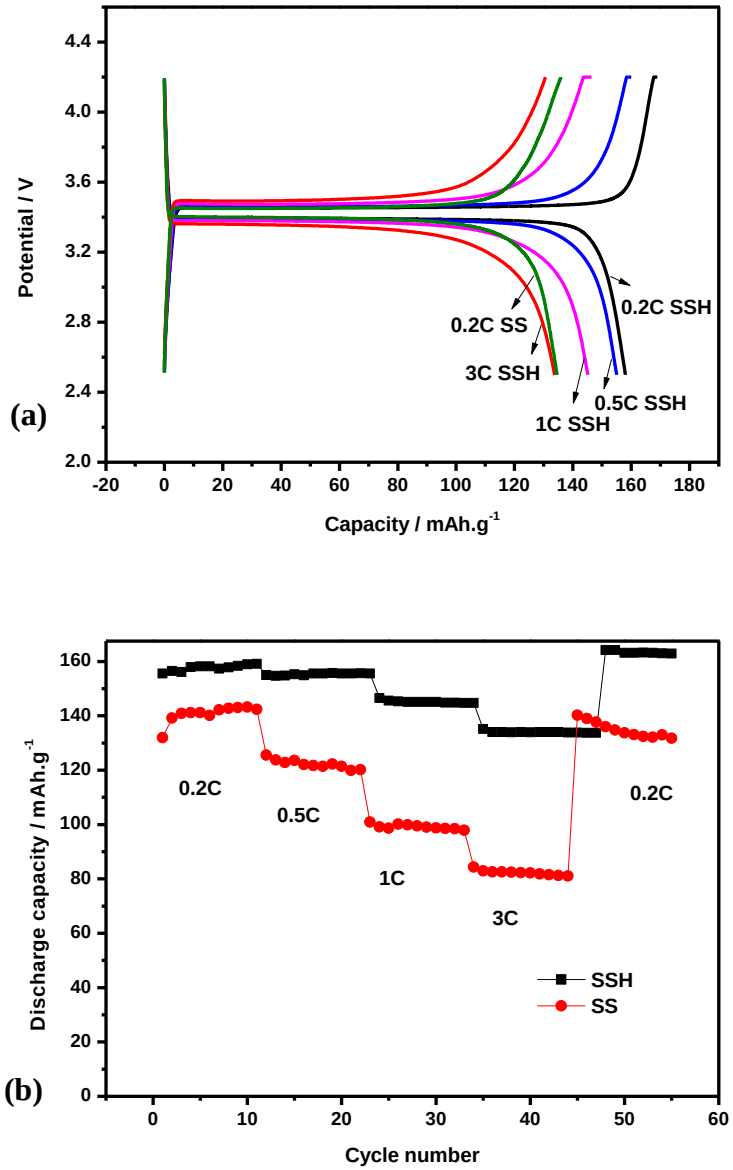

Figure 6. (a) Typical charge/discharge behaviors and (b) Cycling capabilities of the samples between 2.5 V and 4.2 V at various current rates.

The broad D and G bonds in the Raman spectrum in Fig. 5 resolved into four peaks at around 1194 cm^{-1}, 1340 cm^{-1}, 1510 cm^{-1}, and 1585 cm^{-1} by following a standard peak de-convolution procedure [9]. The bands at 1194 cm^{-1}, 1340 cm^{-1}, and 1510 cm^{-1} were assigned to tetrahedral and sp^3-type carbons. Thus, the ratio of sp^3 bonds to sp^2 G-bond (1585 cm^{-1}) and *R* can be calculated (Table 1).

Table 1. Characteristic parameters of the samples obtained by fitting of the Raman spectra

	SS	SSH
$R\ (I_G/I_D)$	1.13	1.18
sp^3/sp^2	3.54	2.37

The carbon in the SSH sample contains more sp^2-type carbon and shows a slightly higher *R* than that in the SS sample. More sp^2-type carbon domains and less disorder in graphene planes enhanced electronic conductivity, which means the carbon derived from HEC-sucrose is superior to the carbon produced solely from sucrose.

The charge/discharge characteristics of the first cycle and the cyclic performance of the SS and SSH electrodes at different C rates are shown in Figs. 6a and Fig.6b. All of the samples displayed flat, long charge and discharge voltage plateaus around 3.5 V and 3.4 V at a rate of 0.2 C, respectively. The capacity dropped with increasing C rate, indicating that the capacity loss was restricted by lithium-ion diffusion.

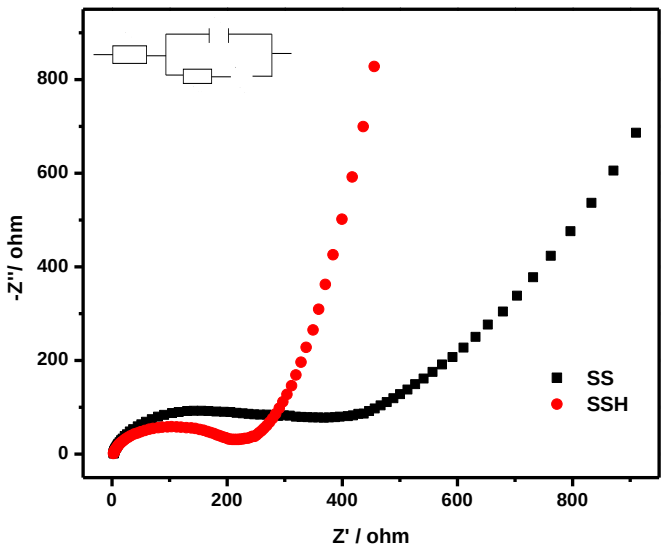

Figure 7. Impedance spectra of coin cells composed of SS and SSH composites. The inset plot is the equivalent circuit.

The SSH electrode sample exhibited 162 mAh g^{-1}, 158 mAh g^{-1}, 148 mAh g^{-1}, and 135 mAh g^{-1} at the charge/discharge rates of 0.2 C, 0.5 C, 1 C, and 3 C, respectively. The capacity of the SS

electrode decreased to 136 mAh g^{-1} at a discharge rate of 0.2 C. The cyclic performance of the SSH electrode is also apparently better than that of the SS samples. However, the capacity drop of the SSH sample across different C rates is smaller, indicating that the electrode polarization is smaller in the SSH sample due to the improved electronic conductivity and carbon coating, which can improve the reversibility of Li-ion insertion/extraction. In addition, the SSH sample showed excellent capacity retention ability, indicating that the carbon coating formed a barrier to avoid corrosion from the electrolyte, especially from HF. EIS was carried out on coin cells composed of SS and SSH composites after 10 cycles at 0.1 C to further understand the effect of HEC addition on the charge transfer. The results are shown in Fig. 7. The EIS profiles consist of a depressed semicircle in the high-frequency region and an inclined line in the low-frequency region. The equivalent circuit is also provided as the inset plot. R_s refers to the resistance of the electrolyte. The particle–particle contact resistance and the resistance between the electrode and current collector are also included in R_s. R_{ct} refers to the charge transfer resistance due to the electrochemical reaction that occurs at the electrode–electrolyte, as well as at the particle–particle, interface. The Warburg impedance (inclined line, labeled as Z_w in the plot) is ascribed to lithium-ion diffusion.

The R_{ct} of the SSH sample is lower than that of the SS sample, indicating the faster electrochemical reaction of the SSH sample. The R_{ct} can be obtained from the intersection of the semicircle with the real axis at the lower frequency side. The smaller R_{ct} can be ascribed to the homogenous particles and superior performance of the pyrolytic carbon from HEC-sucrose.

The appropriate amount of carbon coated on a sample can improve its electrochemical properties [22]. However, the carbon from different carbon-containing compounds confers varying performance. Choosing the appropriate carbon precursor is very important in obtaining a $LiFePO_4$/C composite with excellent properties. In this work, we found that HEC-sucrose could be used as an appropriate carbon precursor, given the beneficial effects of pyrolytic carbon to the $LiFePO_4$ particles, including improved carbon structure, increased homogeneity of the resulting grains, and uniformity of the coated carbon layer on the particles.

4. CONCLUSIONS

In summary, carbon-coated $LiFePO_4$ powder was prepared via an HEC-assisted rheological phase method using custom-made $FePO_4$ as the iron source. Characterization data collected by XRD, SEM, and TEM, as well as Raman spectra, reveal that the addition of HEC is effective in obtaining homogeneous particles and a uniform carbon layer on the particles. The HEC-sucrose complex can form more graphite-like carbon during pyrolysis, providing the $LiFePO_4$/C sample with higher capacities and better rate capability. The $LiFePO_4$/C sample obtained from HEC-containing precursors also exhibits a smaller total resistance because of well-dispersed particles and a uniformly coated carbon layer.

ACKNOWLEDGEMENT
This work was financially supported by the Development and Reform Commission of Guangdong Province (No.301-5).

References

1. A.K. Pahi, K.S. Kanjundaswamy, J.B. Goodenough, *J. Electrochem. Soc*. 144 (1997) 1188.
2. D. Lepage, C. Michot, G.X. Liang, M. Gauthier, S.B. Schougaard, *Angew. Chem. Int*. Ed. 50 (2011) 6884.
3. S. Kandhasanmy, A. Pandy, M. Minakshi, *Electrochim. Acta* 60 (2012) 170.
4. D. Morgan, A. Vanderven, G. Ceder, *Electrochem. Solid State* 7 (2004) A30.
5. P. Axmann, C. Stinner, M. Wohlfahrt-Mehrens, A. Mauger, F. Gendron, C.M. Julien, *Chem. Mater*. 21 (2009) 1636.
6. R.R. Zhao, I.M. Hung, Y.T. Li, H.Y. Chen, C.P. Lin, *J. Alloys Compd*. 513 (2012) 282.
7. K. Wang, R. Cai, T. Yuan, X. Yu, R. Ran, Z.P. Shao, *Electrochim. Acta* 54 (2009) 2861.
8. Z.G. Lu, H. Cheng, M.F. Lo, C.Y. Chung, *Adv. Funct. Mater*. 17 (2007) 3885.
9. G.T.K. Fey, H.J. Tu, K.P. Huang, Y. C. Lin, H.M. Kao, S.H. Chan, *J. Solid State Electrochem*. 16 (2012) 1857.
10. N.Ravet, M. Gauthier, K. Zaghib, J.B. Goodenough, A. Mauger, F. Gendron, C.M. Julien, *Chem. Mater.* 19 (2007) 2595.
11. W.X. Peng, L. F. Jiao, H.Y. Gao, Z. Qi, Q.H. Wang, H.M. Du, Y.C. Si, Y.J. Wang, H.T. Yuan, *J. Power Sources* 196 (2011) 2841.
12. K.R. Yang, Z.H. Deng, J.S. Suo, *J. Power Sources* 201 (2012) 274.
13. K. Kim, Y.H. Cho, D. Kam, H.S. Kim, J.W. Lee, *J. Alloys Compd* 504 (2010) 166.
14. J.H. Hong, Y.F. Wang, G. He, M. Z. He, *Mater. Chem. Phys*. 133 (2012) 573.
15. S.W. Oh, S.T. Myung, S.M. Oh, K.H. Oh, K. Amine, B. Scrosati, Y.K. Sun, *Adv. Mater*. 22 (2012) 4842.
16. Y.Q. Wang, J.L. Wang, J. Yang, Y. Nuli, *Adv. Funct. Mater*. 16 (2006) 2135.
17. S.J. Kwon, C.W.Kim, W.T. Jeong, K.S. Lee, *J. Power Sources* 137 (2004) 93.
18. D.H.Kim, J.Kim, *J. Phys. Chem. Solids* 68 (2007) 734.
19. J.J. Chen, M.S. Whittingham. *Electrochem. Commun*. 855.
20. R.R. Zhao, L.C. Zhu, Z.Z. Huang, J.Z. Liang, H.Y. Chen, *Ionics* DOI: 10.1007/s11581-012-0799-4.
21. V. Palomares, A. Goñi, I. Muro, I. Meatza, M. Bengoechea, I. Cantero, T. Rojo, *J. Power Sources* 195 (2010) 7661.
22. H. Huang, S.C. Yin, L.F. Nazar, *Electrochem. Solid State* 4 (2001) A170.